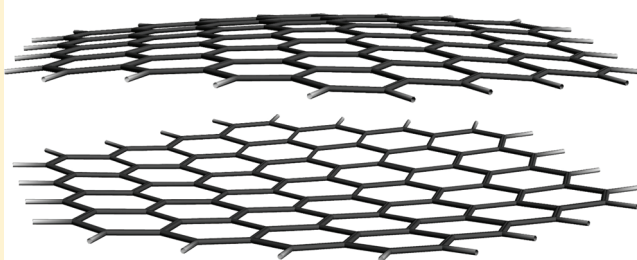# On the Nature of Interlayer Interactions in a System of Two Graphene Fragments

Julia Berashevich* and Tapash Chakraborty

Department of Physics and Astronomy, University of Manitoba, Winnipeg, Canada R3T 2N2

ABSTRACT: With the help of the quantum chemistry methods, we have investigated the nature of interlayer interactions between graphene fragments in different stacking arrangements (AA and AB). We found that the AB stacking pattern, as the ground state of the system, is characterized by the effective interband orbital interactions which are barely present in the AA. Their vanishing induces electronic decoupling between the graphene layers, so that the bonding interaction ΔE_{oi} between the flakes is drastically reduced from -0.482 to -0.087 eV as the stacking pattern is changed from AB to AA. The effective way to improve the bonding interaction between layers preserving the same AA lattice order is to induce rotation of the layer.

Buckling of bilayer graphene

As the flake is rotated, the bonding interactions are improved mostly due to suppression of the Pauli repulsion which in turn increases the interlayer orbital interactions, while the interband part of those remain negligible on the whole range of the rotation angle. The Pauli repulsion is also found to be the main force that moves the two fragments apart as the stacking pattern is changed from AA to AB. This enhances the equilibrium interlayer distance, which for the AA staking is larger than the established value for the AB stacking (3.4 Å).

I. INTRODUCTION

Bilayer graphene,[1−9] regarded as an important system for applications in semiconductor electronics, has intrigued the scientific community to look deeper into the nature of interlayer interactions in this system. Graphene layers stacked together are uniquely different from other solid state materials because of the interlayer weak van der Waals and steric interactions, instead of the occurrence of C−C bonding between the layers. The half-filled p orbital left on each carbon atom after bonding with its neighbors within the honeycomb lattice is responsible for formation of the π bonds between two neighboring atoms within the same layer. This creates a closed shell electron system carrying the weakly bound π electrons that are distinct due to their high mobility within the graphene layer.[10−12] Stacking two systems of closed electron shells would cause the interlayer interactions to be mostly repulsive which results in the expulsion of valence electrons from the overlap region such that only a weak electronic coupling between the layers can occur. If under certain conditions the electronic coupling becomes negligible then each layer would display its own electronic behavior in the band diagram as was found recently in twisted bilayer graphene.[7,8,13]

Even before the discovery of graphene, the interlayer interactions in natural graphite, which is basically a system of stacked graphene layers, received intense attention[14−17] where the effect of interlayer decoupling was not encountered. Three types of layer arrangements are known to exist in graphite,[14] but the most common one is the Bernal stacking in which the carbon atoms belonging to different sublattices A and B form the AB stacking pattern between the layers (atoms belonging to A sublattice in

one layer are stacked directly above the atoms of B sublattice from another layer). Contrary to the conventional wisdom that only the long-range van der Waals interaction is important in the case of stacking of closed shell systems, for the AB stacking in graphite, it was shown that the orbital overlap between the π orbitals belonging to different layers[15,18] is as essential as the all important van der Waals forces. Therefore, it was predicted that despite the well-known interlayer distance of 3.4 Å in natural graphite, for a system containing only two or three layers, the interlayer spacing depends on the number of layers[15] due to different nodal interactions of the overlapping π orbitals. For an odd number of adjacent layers, the equilibrium spacing between the layers was predicted to be 3.30 Å, whereas for the even number, it is 3.58 Å.[15] It then clearly follows that in graphite the electronic coupling between the layers can not be neglected. Rather, it provides a substantial influence on the interlayer interactions in addition to the van der Walls and steric type of interactions.

In this context, it is worth pondering what is actually happening with the interlayer interactions in twisted bilayer graphene where, interestingly, one observes electronic decoupling between the layers. The decoupling was first observed experimentally[1−3] and was later investigated theoretically.[7,8,13] Theoretical interpretations[7,8,13] relate the decoupling to the occurrence of a misorientation of 2−5° between the layers. According to a proposed model, the layer rotation in the real space induces a displacement

of the Dirac cones generated in each layer in the reciprocal space[7,8,13] thereby causing the interlayer decoupling. Experimentally, the misorientation of 2—5° in AA-stacked bilayer graphene has been detected in systems that were created using various fabrication techniques such as the epitaxial growth,[1–3] chemical vapor deposition[4] and ultrasonication.[5] The AA stacking is refereed to the system in which atoms belonging to the same sublattice are stacked directly on top of each other. Appearance of the rotational misorientation that is independent of the fabrication techniques suggests the presence of some forces between the layers strong enough to cause the layer rotation. However, the available theoretical models[7,8,13] on the electronic properties of the AA stacked graphene deal only with the band properties but do not shed any light on the underlying reasons involved in decoupling, such as the interlayer forces.

In a recent work[18] we related the origin of the decoupling phenomenon and rotational misorientation with layer stacking pattern which is AA in fabricated multilayer graphene[1–5] against the AB stacking in natural graphite. For the AA staking, the interlayer electronic coupling is suppressed by a significant repulsion arising between the graphene layers.[18] This repulsion is also expected to be responsible for the occurrence of lattice misorientation between the layers. It was suggested that rotational misorientation, which creates the Moiré pattern, appears as a way to suppress the repulsion, thereby lowering the total energy of the system. Even a slight layer rotation of ∼2°-5° substantially shrinks the areas characterized by the AA lattice superposition in which repulsion dominates over other forces (the areas with AA and AB stacking coexist in the Moiré pattern). The other important result was a prediction[18] that the strong repulsion may induce bumps on the graphene surface in the areas where AA stacking is preserved. All these effects are important and require careful studies because the phenomenon of layer rotation through electronic coupling between layers can offer ways to manipulate the electronic properties of twisted graphene (Moiré pattern of different rotation angle is characterized by different percentage of AA-spotted areas). Therefore, in this work we present a detailed quantitative analysis of the repulsive forces and the orbital overlap in stacked graphene layers and their alteration with the appearance of rotation. Our studies are based on the density functional methods including a recently proposed empirical correction (Grimme correction[19]) which was developed for a proper consideration of the dispersive interactions between the closed shell electron systems.

II. COMPUTATIONAL METHODS

The computations were performed with the ADF quantum chemistry code[20] which uses the Kohn—Sham approach to density functional theory (DFT). The Kohn—Sham approach replaces the many-body system within the Hamiltonian equation by a system of the noninteracting particles while all the many-body terms are incorporated into the so-called Kohn—Sham potential. This concept is quite useful in the investigation of interacting closed shell systems because it allows us to present each graphene flake as an isolated fragment and two fragments interact as the flakes are stacked. In this way, a proper investigation of the forces and the orbital overlap can be performed directly in terms of the fragment presentation.

Within the ADF code the forces between fragments are included in the bonding energy ΔE^0 which comprises of several majors components[21] ($\Delta E^0 = \Delta V_{el} + \Delta E_p + \Delta E_{prep} + \Delta E_{oi} + E_{dis}$).

The first component (ΔV_{el}) takes care of the interactions of electrostatic nature related to the modification of the charge distribution (originated from the charge transfer between occupied and unoccupied orbitals), when two systems are allowed to interact. The second one is the energy change induced by the Pauli repulsion (ΔE_p), which include several components: exchange repulsion, kinetic repulsion, overlap repulsion, all results from obeying the Pauli antisymmetry principle. The next term ΔE_{prep} describes the energy required to change the conformation of the fragments (structural modification) from the initial geometry containing separate fragments to the final geometry where the fragments are allowed to interact. The bonding interactions between two fragments are included in the ΔE_{oi} term which originates from the overlap of the fragment's orbitals. The last term E_{dis} is the empirical dispersion correction introduced by Grimme[19] and its magnitude is defined by the long-range van der Waals interactions, whose contribution in the short-range is reduced by the damping function.

Even though the ΔE_{oi} term is a measure of the orbital overlap, the interlayer forces such as the Pauli repulsion and orbital polarization contribute to the ΔE_{oi} as well. The effect of interlayer forces can not be discarded from ΔE_{oi} and so the overlap of the selected orbitals can not be separated from the others. This makes it hard to get a proper understanding of the intricacies of interlayer interactions between two fragments. The most effective way to proceed is to follow the established method of linear combinations of the orbitals. This method can be applied for the results obtained with the ADF program. With the ADF, each fragment is described by its own set of orbitals and the program facilitates their mixing upon the inclusion of the interaction between the fragments. Therefore, the fragment approach allows us to evaluate the overlap matrix $S_{i,j}$ between the fragments i and j of the Kohn—Sham Hamiltonian ($\langle\varphi_i|h_{KS}|\varphi_j\rangle$) directly in terms of the linear combinations of the fragment orbitals via the relation $h_{KS} = SCEC^{-1}$, where C is the eigenvector defined in terms of the fragment orbitals and E is the eigenvalue matrix.[22] The overlap matrix S purely depends on the form of the interacting orbitals and on the distance that keeps the two fragments apart neglecting the contribution from the attractive and repulsive forces arising between the fragments. We used the overlap matrix $S_{i,j}$ to define the spatial overlap integral between the fragments i and j, which is $J_{i,j} = \langle\varphi_i|H|\varphi_j\rangle$.

In this work we consider the spatial overlap integral $J_{i,j}^{H-H}$ between the highest occupied fragment orbitals (HOFO), i.e., between two π orbitals, each located on different fragments while their overlap defines the HOMO of the joint system. The overlap integral was also calculated between the π and π^* orbitals, i.e., between the highest occupied orbital of one fragment (HOFO$_1$) with the lowest unoccupied orbital of another fragment (LUFO$_2$) and because there are two parts of such interactions, HOFO$_1$—LUFO$_2$ and HOFO$_2$—LUFO$_1$, the average value of overlap integral was considered and combined into the $J_{i,j}^{H-L}$.

We used the hybrid BLYP exchange-correlation functional, applying the empirical dispersion correction 1.05 recommended by Grimme.[19,23] For the interacting molecules of closed electron shells it was found that the proposed correction is enough to reproduce the intermolecular distance to what is observed in the experiments or achieved with a more accurate level such as the ab initio Møller—Plesset second-order (MP2) method.[19] For a proper description of the tails of the electron wave functions that is important for long-range interactions, we used the Slater-type orbitals. The quite extended TZP basis set
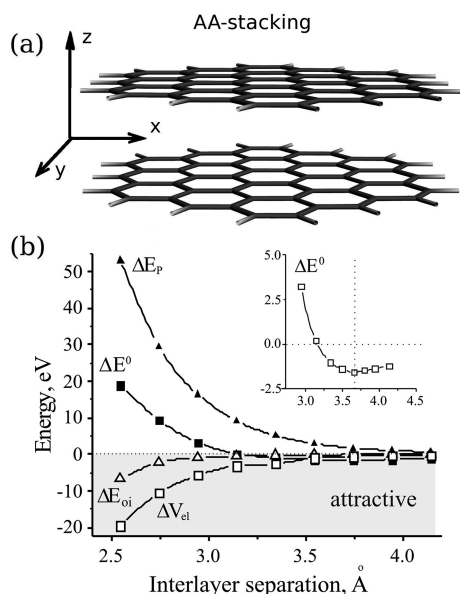
Figure 1. (a) Graphene flakes stacked in AA conformation in the 3D space coordinate system. (b) The energy components (ΔV_{el}, ΔE_p, and ΔE_{oi}) of the bonding energy (ΔE^0) as a function of the interlayer distance between two graphene fragments of AA stacking order. ΔV_{el} is the electrostatic interactions, ΔE_p is Pauli repulsion, and ΔE_{oi} is the orbital interactions energy.

Table 1. Electronic Properties and the Interlayer Forces between Two Graphene Fragments Stacked in AA ($d_{eq(AA)}$ = 3.67 Å), in AB ($d_{eq(AB)}$ = 3.4 Å), and in AA′ ($d_{eq(AA)}$ = 3.41 Å) Configurations[a]

	HOMO	LUMO	$J_{i,j}^{H-H}$	$J_{i,j}^{H-L}$	ΔE_{oi}	ΔV_{el}	ΔE_p	ΔE^0
AA	−4.024	−2.596	0.443	10^{-5}	−0.087	−0.691	2.136	−1.483
AB	−4.164	−2.506	−0.229	−0.169	−0.482	−1.184	3.388	−1.931
AA′	−4.070	−2.565	0.023	−0.191	−0.491	−1.263	3.644	−1.863

[a] All values are in eV.

(triple-ζ polarized basis set) was applied in all the calculations which improves the precision of our results while suppressing the basis set superposition error.[24] We tested the chosen method to reproduce the interlayer distance between the graphene flakes stacked in the AB pattern (which is well-known to be 3.4 Å in natural graphite) and indeed the correct interlayer distance was obtained (the so-called equilibrium distance of the AB pattern $d_{eq(AB)}$). For this calculation the atomic coordinates within the graphene plane (along the x,y directions) were confined and only the coordinates in the z direction, i.e., perpendicular to the graphene plane, were used for relaxation. In fact, the full relaxation of the system of two stacked fragments is problematic as the repulsion between layers leads to sliding of the fragments away from each other.

Our main emphases in this work are the energy decomposition analysis of the bonding energy ΔE^0 (ΔV_{el}, ΔE_p, ΔE_{prep}, and ΔE_{oi}) and the spatial overlap integrals ($J_{i,j}^{H-H}$, $J_{i,j}^{H-L}$) which are determined by the stacking pattern between two graphene flakes (flake rotation) and the interlayer distance. In most cases the single point calculations have been used for which the contribution of ΔE_{prep} becomes zero.

III. AA AND AB STACKING

For our investigations we used two graphene flakes with the carbon atoms at the edges terminated by the hydrogen atoms, as shown in Figure 1a with our goal to minimize the contribution of the edge localized states into the simulation results. Because bilayer graphene obtained in the experiments[1−3] has shown the AA stacking pattern instead of the AB, common in natural graphite, we probe the AA stacking for the equilibrium distance between the flakes ($d_{eq(AA)}$). It was found that this distance is indeed enhanced in the AA stacking up to $d_{eq(AA)}$ = 3.67 Å against the $d_{eq(AB)}$ = 3.4 Å for the AB stacking. To explain an

increase in the interlayer distance, we applied the decomposition analysis of the bonding energy.

We performed the single point calculations in which the layers were separated by the established equilibrium distances (d_{eq}) found to be different for AA and AB stacking. The obtained interlayer forces and spatial overlap integrals are collected in Table 1. For the purpose of comparison, in addition to the lattice arrangements AA and AB, we also carried out the bonding analysis for the AA′ stacking pattern for which the interlayer equilibrium distance was found to be 3.41 Å and those results are also displayed in Table 1. According to the obtained HOMO and LUMO energies, the HOMO−LUMO gap is around 1.5 eV. Such a large value is expected from the confinement effect[25] which appears for graphene structure of finite size. An increase in the flake size will lead to an exponential reduction of the gap,[26] whereas making graphene infinite in one or two directions leads to disappearance of the gap.

The AB conformation is characterized by a much stronger bonding interaction than that of AA, as defined by a more negative bonding energy ΔE^0, thereby making the AB stacking the ground state of the system. The structural distinction of the AB configuration from AA consists in sliding of one graphene flake relative to the other by 1.42 Å along the x axis that induces the shift of the bond positions between the layers against their superposition for the AA stacking (for the AA case the atomic coordinates are matched in the x and y directions for both layers). To obtain the AA′ stacking, a sliding of 1.23 Å is applied along the y axis.

For the AA stacking, due to the lattice superposition the π clouds between the layers are also superposed that leads to their effective overlap defined by the spatial overlap integral $J_{i,j}^{H-H}$ = 0.443 eV. The flake sliding induced for the AB and AA′ stacking breaks the bond superposition condition recognized for the AA stacking thereby inducing the disarrangement of the π clouds within the overlapping region. As a result, the $\pi-\pi$ interlayer interactions, which is of particular interest since it is supposedly responsible for the occurrence of electronic coupling between the graphene layers,[9,27] is significantly reduced for the AB stacking pattern. This is reflected by a suppression of the spatial overlap integral to $J_{i,j}^{H-H}$ = −0.229 eV (even more drastic reduction is observed for the AA′ case where $J_{i,j}^{H-H}$ = 0.023 eV).

When two fragments are stacked, the majority of the orbital interactions described by ΔE_{oi} arise from the overlap of the π orbitals ($\pi-\pi$ or $\pi-\pi^*$). For interaction of two closed shell systems, the $\pi-\pi$ overlap is not the one that leads to the bonding interactions and, therefore, might be ignored within the orbital interaction term ΔE_{oi}. That explains the contradictory behavior of the overlap integral $J_{i,j}^{H-H}$ and the ΔE_{oi} term, such that when a reduction of the overlap integral $J_{i,j}^{H-H}$ occurs for the AB stacking, the orbital interactions ΔE_{oi} between the fragments is improved.
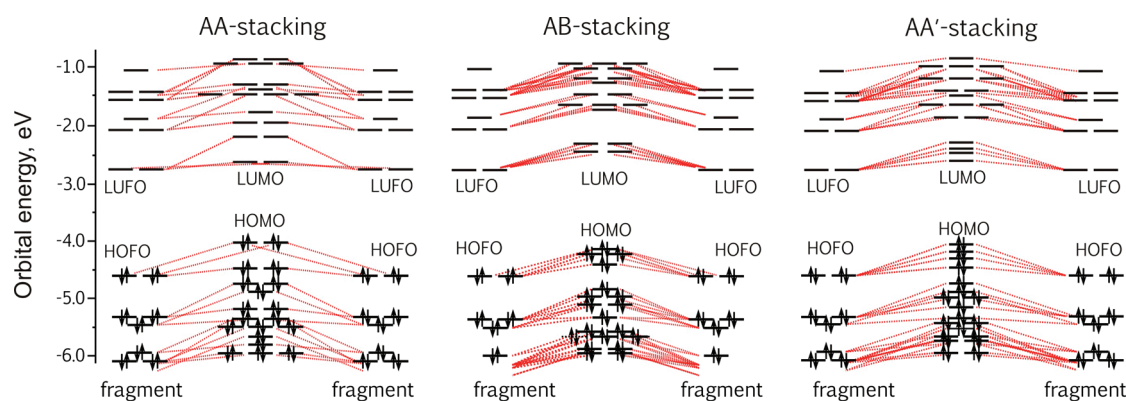
Figure 2. Energy diagram demonstrating the formation of the molecular orbitals (HOMOs and LUMOs) as the fragment's orbitals overlap (HOFO and LUFO) for different arrangements of graphene lattices when the fragments are separated by the equilibrium distance d_{eq}.

However, the improvement of ΔE_{oi} with modification of the lattice arrangement from AA to AB is also not consistent with behavior of the Pauli repulsion ΔE_p whose increase supposedly suppresses the interlayer orbital interaction ΔE_{oi}. Therefore, to understand the alteration of the ΔE_{oi} term we should take into consideration other components of the orbital interactions, such as the orbital polarization and the interlayer interaction of the $\pi-\pi^*$ orbitals.

Orbital polarization reflects a mixing of the occupied/virtual orbitals in one fragment due to the presence of another fragment; that is, each valence electron of one fragment entering the electron space of electrons of other fragment polarizes its orbitals. The polarization effect is caused by the repulsion arising between interacting electrons.[28] Analyzing the orbital formation after perturbation of the fragment's orbitals, a discrepancy in the product orbitals for the AB, AA, and AA′ stacking patterns was detected as demonstrated by the scheme in Figure 2. Let us consider the formation of the orbitals generating the HOMO−LUMO gap in the joint system which would give the most contribution into the interlayer interaction of the $\pi-\pi^*$ orbitals. In formation of HOMO orbital (LUMO) of the joint system two degenerate fragment's orbitals HOFO participates (two LUFO orbitals for the LUMO formation). Perturbation of those degenerate HOFO orbitals (overall four in two fragments) creates the four molecular orbitals in the bilayer system (HOMO, HOMO−1, HOMO−2, and HOMO−3). Similarly, the LUFO orbitals perturb in the conduction band so that two LUFOs are taken from each fragment and their perturbation leads to formation of four LUMO orbitals in the stacked system (LUMO, LUMO+1, LUMO+2, and LUMO+3). For the AA stacking, two pairs of product orbitals possess an identical orbital energy, i.e., HOMO and HOMO−1 (LUMO and LUMO+1) are degenerate, the same for HOMO−2 and HOMO−3 (LUMO+2 and LUMO+3). However, already for the AB case the conduction band is limited by a single HOMO orbital being a product of the perturbation of all four fragment's orbitals while the rest of the generated orbitals are shifted deeper into the conduction band where two of them still would remain degenerate. Mixing of the LUFOs for the AB stacking stays similar to those for the AA case, i.e., two pairs of the degenerate orbitals are formed. For the AA′ stacking all four product orbitals HOMOs (LUMOs) are separated by the energy gap.

The spatial orbital overlap $J_{i,j}^{H-H}$, regardless of the observed peculiarities of orbital mixing as lattice arrangement is changed, is

being affected mostly by rearrangements of the π clouds from their superposition in AA stacking. However, an analysis of interaction of the occupied/unoccupied orbitals between fragments $J_{i,j}^{H-L}$ has shown a distinct behavior. We observed weak overlap between those orbitals in the AA pattern ($J_{i,j}^{H-L} = 10^{-5}$ eV), while it appears for the AB stacking to be 0.169 eV and increases even further up to 0.191 eV for the AA′ stacking. Such progress is consistent with an improvement of the orbital interactions ΔE_{oi} and with enhancement of the attractive interactions of the electrostatic nature (see ΔV_{el} in Table 1) as stacking pattern is changed from AA to AB. The terms ΔE_{oi} and ΔV_{el}, lower the bonding energy ΔE^0 and their contributions compensate the growing Pauli repulsion between the fragments.

Therefore, the efficiency of the acceptor−donor interactions, defined by ΔE_{oi}, is found to be several times (at least five) weaker for the AA stacking in comparison to that for the AB. This behavior offers an interpretation of the interlayer decoupling observed in the experiments for the AA stacking in twisted bilayer graphene,[1−5] against the efficient coupling known for the AB stacking. According to our findings the interlayer decoupling in AA staking must be caused by suppression of the orbital overlap of the occupied (π) and unoccupied (π^*) orbitals between the fragments, i.e. interband (HOMO−LUMO) interaction, while a variation of the $\pi-\pi$ overlap is found to have a insignificant affect on the interaction between fragments. This conclusion is, in fact, in contrast to the commonly accepted opinion that the electronic coupling between the stacked graphene layers, which is capable to change linear Dirac cones dispersion to parabolic one, originates from intraband interlayer interactions.[9,27] We should also note that along with the intra- and inter-band interactions the effect of orbital polarization is one of the significant contribution into the bonding interactions.

IV. INTERLAYER DISTANCE

The observation that the interlayer repulsion characterized by ΔE_p is being stronger for the AB stacking in comparison to that for AA was contrary to our expectations because the Pauli repulsion is presumed to dominate when one structure of closed electron shell is placed exactly on top of the other (such as the coordinates in $x-y$ directions coincide as presented in Figure 1a). The Pauli repulsion has the exponential dependence on the separation distance and an increase in d_{eq} for the AA case must cause a significant suppression of the repulsive forces. To understand
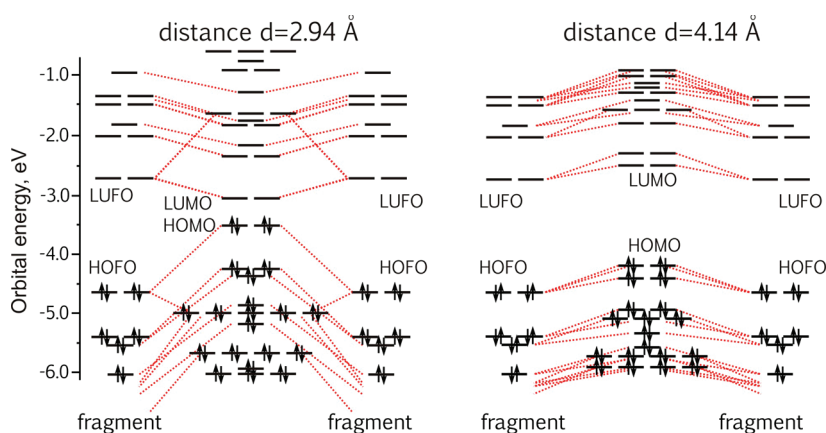
24669

dx.doi.org/10.1021/jp2095032 |*J. Phys. Chem. C* 2011, 115, 24666–24673

Figure 3. Energetics of the π and π^* orbitals defining the HOMO−LUMO gap in the separated fragments and their splitting as fragments being stacked in the AA lattice arrangement.

this, we considered the deviation of the bonding energy and its components with the change in the interlayer distance for the AA stacking [Figure 1b]. The negative sign is for the attractive interactions. The electrostatic interactions ΔV_{el} and the orbital interactions ΔE_{oi} are both attractive in nature and their magnitudes are reduced with increasing distance between the fragments (ΔV_{el} can have a positive magnitude only for short interlayer distance when the nuclear repulsion dominates over other attractive terms). The contribution of the repulsive forces collected within ΔE_p into the total bonding energy displays its domination over the attractive terms only for a short interlayer distance, so the ΔE^0 remains positive (repulsive) up to a distance of 3.2 Å. The bonding energy ΔE^0 reaches its minimum at $d_{eq} \approx$ 3.67 Å ($\Delta E^0 \approx -1.48$ eV) which is still energetically far from the ground state of AB stacking, where $\Delta E^0 = -1.93$ eV.

Among all of the interaction terms, the Pauli repulsion and the bonding interactions are of particular interest. According to the Pauli principle the valence electron from one fragment is not supposed to penetrate the closed valence shell of the other fragment because the repulsive forces expel the charges from the overlap region. The main component within ΔE_p which contribute to the repulsion effect comes from the kinetic energy while the potential energy part is attractive.[21] It is noticeable in Figure 1b that as the fragments being separated at a distance beyond the value of 4.0 Å the Pauli repulsion becomes negligible. However, if we compare the AA and AB stacking for the same interlayer distance 3.4 Å, the Pauli repulsion is larger by almost 1.0 eV for the AA stacking (for AA and AB stacking $\Delta E_p = 4.33$ and 3.38 eV, respectively), in agreement with our expectations, as stated above.

The orbital interaction energy ΔE_{oi} belongs to the attractive forces and its value reflects the efficiency of the donor−acceptor charge transfer between fragments which is controlled by the interlayer orbital overlap together with the Pauli repulsion and orbital polarization. Suppression of the Pauli repulsion with growing interlayer distance tends to increase the orbital interaction energy ΔE_{oi}. However, a simultaneous reduction of the spatial orbital overlap generally leads to diminishing of ΔE_{oi}, i.e., to a reduction of the charge transfer between the fragments. As a result, ΔE_{oi} being strongly attractive (negative sign) at short distances almost vanishes as the distance reaches the value of $d \simeq$ 3.3 Å, whereas after $d \simeq 3.9$ Å, it turns repulsive with a positive sign. It was noticed that the composition of the molecular orbitals

Table 2. Spatial Overlap Integral $J_{i,j}^{H-H}$ and $J_{i,j}^{H-L}$ and HOMO−LUMO Gap ΔE_{gap} Calculated for the AA Stacking Pattern as the Flake Separation d Gradually Increases[a]

d	2.94	3.14	3.34	3.40	3.54	3.74	3.94	4.14
$J_{i,j}^{H-H}$	−1.21	−0.91	−0.68	−0.63	−0.51	−0.38	−0.28	−0.21
$J_{i,j}^{H-L} \times 10^{-5}$	5.03	3.52	2.54	1.62	1.31	1.09	0.86	0.61
ΔE_{gap}	0.45	0.84	1.13	1.20	1.34	1.50	1.61	1.69

[a] All values are in eV.

near the HOMO−LUMO gap is not changed with distance as it is shown in Figure 3. For example, HOMO is formed as the orbital overlap of HOFO provided by each fragment and remains of the same composition independent of distance change while just become shifted in energy due to the modification of the interlayer forces. Therefore, we can conclude that the orbital polarization term brings no contribution in deviation of ΔE_{oi} with distance.

To separate the orbital interactions from other forces, we calculated the spatial overlap integral between the fragments $J_{i,j}^{H-H}$ and $J_{i,j}^{H-L}$. The degradation of $J_{i,j}^{H-H}$ upon increase of the interlayer distance along with the size of the HOMO−LUMO gap (ΔE_{gap}) are presented in Table 2. Because a rise in interlayer separation d induces a suppression of the orbital overlap, in particular of the overlap matrix $S_{i,j}$, the charge transfer integral $J_{i,j}^{H-H}$ is also being reduced. The same gradual reduction is observed for the $J_{i,j}^{H-L}$ overlap (from 5×10^{-5} to 6×10^{-6} eV).

As one increases the interlayer distance d the HOMO−LUMO gap grows in contrast to the diminishing $J_{i,j}$ and its enhancement is directly connected to the orbital interaction between the fragments. We presented in Figure 3 the energy diagram for the energetics of the π and π^* orbitals near the HOMO−LUMO gap for the case of separated fragments and their orbital splitting/mixing after perturbation. To find the orbital energy change by the fragment interaction we used the expression derived within the Hückel approximation for the description of splitting of the π orbitals belonging to different fragments after inclusion of the interactions

$$E_1 \approx e_0 + H_{12} - (e_0 + H_{12})S_{12} \qquad (1)$$

$$E_2 \approx e_0 - H_{12} + (e_0 - H_{12})S_{12} \qquad (2)$$

where e_0 and $E_{1,2}$ are the molecular π-orbital energies before (for identical graphene flakes $e_1 = e_2 = e_0$) and after perturbation,

respectively. S_{12} is the orbital overlap between the fragments and H_{12} is the intrinsic interaction integral that is a combination of the energy terms responsible for electron−electron interactions and particularly the contribution of its repulsive part to the orbital energies $E_{1(2)}$.

As fragments are brought to a distance of 2.94 Å (see Figure 3) which is much shorter than the equilibrium separation (d_{eq} = 3.67 Å), the repulsive force dominates over the attractive interaction. Therefore, since the electrons are expelled by repulsion from the overlap region, within the Hückel approximation the overlap matrix S_{12} is treated as zero or would possess a negative value so that for simplicity, we can ignore the contribution from $(e_0 \pm H_{12})S_{12}$ to the orbital energy $E_{1(2)}$. Besides the effect of repulsion on $(e_0 \pm H_{12})S_{12}$ term, the strong repulsion between the fragments causes the increment of the H_{12} and therefore, closer the fragments are to each other the larger the splitting of their π orbitals. The significant $\pi-\pi$ splitting leads to shift of the LUMO and HOMO orbitals close to each other thus causing a suppression of the HOMO−LUMO gap. However, for a large interlayer distance of 4.14 Å, the value of H_{12} diminishes because of the suppression of the Pauli repulsion, while the overlap matrix would have positive values. The charge exchange between the fragments is allowed which decreases the splitting $|E_1 - E_2|$ for the π orbitals and in turn enlarges the HOMO−LUMO gap (ΔE_{gap}).

In this section we considered the basics of the orbital interactions between two graphene fragments when controlled solely by the separation distance. It was understood that there are two main components affecting the efficiency of the orbital interaction energy by varying the distance: the Pauli repulsion and the spatial orbital overlap, while no contribution from the orbital polarization was observed. The spatial orbital overlap decreases with increasing distance and so is the Pauli repulsion. These changes have the opposite influence on the orbital interaction energy ΔE_{oi}, but since the decrease of the spatial orbital overlap is faster than the Pauli repulsion, ΔE_{oi} is generally reduced with induced flake separation.

V. FLAKE ROTATION

For two graphene layers stacked together, the rotational misorientation creates the Moiré pattern which is a periodic pattern manifesting itself through the spots where the superposition of the lattices is preserved, i.e., the AA stacking.[7,8,13] The rest of the surface (the interspot regions) which are of a larger amount of the surface, possesses the stacking order similar or close to that for the AB arrangement (see ref 29 for images of various rotation structures). As the rotation angle increases, the percentage of AA-spotted areas grows while the size of the spots and the interspot areas shrink. Already for angles above 20° the spots with ideal AA stacking vanish completely, leaving the mixed and weakly defined interlayer lattice order. Therefore, the experimentally observed lattice misorientation induced by rotation angle of 3−5° (see refs 1−5) is characterized by the well-defined AA-spots and a high coverage of AB-stacking.

Graphene flakes of finite size are considered in this paper as a model system to represent the spots characterized by the lattice superposition (the AA-spots) in misoriented bilayer graphene. Therefore, by rotating one flake with respect to the other (the rotation axis is placed at the flake center) we basically recreate the modification of the shape of the AA-spots affected by the rotation angle. The main disadvantage of describing misoriented bilayer

Table 3. Interlayer Interactions in the System of Two Twisted Flakes Separated by a Distance d = 3.4 Å[a]

θ	ΔE_{gap}	$|J_{i,j}^{H-H}|$	$|J_{i,j}^{H-L}|$	ΔE_{oi}	ΔV_{el}	ΔE_p	ΔE^0
0.0	1.203	0.627	1.6×10^{-5}	−0.248	−1.423	4.334	−1.195
1.5	1.209	0.604	2.5×10^{-4}	−0.253	−1.421	4.325	−1.207
3.0	1.226	0.544	6.5×10^{-4}	−0.268	−1.416	4.300	−1.242
6.0	1.287	0.563	6.5×10^{-4}	−0.320	−1.399	4.205	−1.368
9.0	1.365	0.305	8.9×10^{-4}	−0.384	−1.376	4.081	−1.530
12.0	1.436	0.116	2.3×10^{-4}	−0.443	−1.356	3.963	−1.682
15.0	1.478	0.131	6.5×10^{-4}	−0.482	−1.342	3.876	−1.790
18.0	1.492	0.061	6.9×10^{-4}	−0.494	−1.335	3.831	−1.837
20.0	1.489	0.176	3.9×10^{-4}	−0.486	−1.333	3.823	−1.832
22.0	1.485	0.318	1.1×10^{-4}	−0.475	−1.332	3.826	−1.816
24.0	1.481	0.184	5.8×10^{-4}	−0.453	−1.333	3.839	−1.779
26.0	1.478	0.344	3.7×10^{-3}	−0.439	−1.333	3.851	−1.753
28.0	1.477	0.363	2.0×10^{-3}	−0.423	−1.334	3.862	−1.724
30.0	1.476	0.322	2.9×10^{-3}	−0.417	−1.335	3.870	−1.713
AB	1.568	0.229	0.169	−0.482	−1.184	3.388	−1.931

[a] For the spatial overlap integral $J_{i,j}^{H-H}$, its modulus has been considered to avoid confusions of the sign change. ΔE_{gap} is the HOMO−LUMO gap in the system of two stacked flakes. For a better comparison we repeated the results for the graphene flakes stacked in the AB pattern at the equilibrium distance d_{eq} = 3.4 Å. All values are in eV.

graphene by finite size flakes is that it underestimates the contribution of the AB stacking areas to the electronic properties of the bilayer system. In the model system of rotated flakes the contribution of the interspot regions with AB stacking would depend on the flake size and therefore for small flakes would be negligible.

In a system of the AA stacked graphene fragments, the interacting π orbitals between the fragments are perfectly orthogonal. The layer rotation observed in the experiments[1−5] breaks that orthogonality, thereby modifying the balance of the attractive and repulsive forces between the layers. We simulated the effect of misorientation in the model system of two graphene flakes presented in Figure 1a with the rotation axis placed at the flake center. In a system of two flakes stacked in the AA pattern and separated by a distance of d = 3.4 Å which is the equilibrium distance for the AB stacking, we rotate one flake relative to the other for further elaboration of the interaction parameters. Our simulation results for the bonding energy ΔE^0 between layers and its components, overlap integrals such as $J_{i,j}^{H-H}$ and $J_{i,j}^{H-L}$, and the HOMO−LUMO gap (ΔE_{gap}) are displayed in Table 3. The results indicate that the size of the HOMO−LUMO gap (ΔE_{gap}) grows as the bonding interaction between layers is improved with rotation.

When two lattices of different flakes are superposed in the space, the electronic clouds of their π orbitals are also superposed giving the maximum magnitude of the overlap integral $J_{i,j}^{H-H}$ which is being suppressed with the flake rotation because of misorientation of those π clouds. Therefore, the spatial overlap integral $J_{i,j}^{H-H}$ reaches its minimum as the rotation angle reaches the value of $\theta \simeq 18°$ which is being a result of significant disarrangement of the π orbitals within the overlapping region from their superposed position. Another overlap integral accounting for interband interactions, $J_{i,j}^{H-L}$ (between HOMO and LUMO orbitals belonging to the different fragments), has shown the opposite behavior to that of $J_{i,j}^{H-H}$, i.e., with its minimum for the superposed case while growing with the flake rotation. However, even when $J_{i,j}^{H-L}$ reaches the maximum at $\theta = 24-30°$, its magnitude

24671

dx.doi.org/10.1021/jp2095032 |*J. Phys. Chem. C* 2011, 115, 24666−24673

is still much lower than that found for the AB stacking. For the angle in the range of $\theta = 24-30°$, both integrals ($J_{i,j}^{H-H}$ and $J_{i,j}^{H-L}$) deviate insignificantly. With breaking of the orthogonality of the π orbitals as the flake is rotated, the Pauli repulsion is also being suppressed by ~ 0.5 eV when its reaches its minimum at $\theta \simeq 18°$. The reduced value of 3.831 eV for $\theta \simeq 18°$ becomes much closer to that for the AB stacking ($\Delta E_p = 3.388$ eV). For the rotation angle $\theta > 18°$, an increase in the Pauli repulsion term suppresses the orbital interaction energy ΔE_{oi} somewhat, despite increasing the magnitude of interband interactions, $J_{i,j}^{H-L}$.

Moreover, the orbital interaction energy ΔE_{oi} grows with flake rotation as the interband interactions reflected by the $J_{i,j}^{H-L}$ improve ($J_{i,j}^{H-L}$ increases up to several orders of magnitude) along with the fast reduction of the interlayer repulsion. The coincidence of the minimum of ΔE_{oi} with the minimum value of the Pauli repulsion achieved for the $\theta \simeq 18°$ is a clear evidence that the efficiency of the orbital interactions is being under direct control of the repulsive forces.

Therefore, because the layer rotation significantly suppresses the interlayer repulsion which in turn improves the orbital interaction, regardless of the deviation of the overlap integrals, the total bonding energy ΔE^0 is lowered with rotation and its magnitude reaches its minimum also at $\theta \simeq 18°$. In fact, the magnitude of the total bonding energy found for the angle $\theta \simeq 18°$ ($\Delta E^0 = -1.837$ eV) is comparable to that for the AB stacking ($\Delta E^0 = -1.931$ eV in Table 1). Above the rotation angle 30°, some fluctuations for all of the terms occur while closer to angle 60° for which the conditions for the lattice superposition between two layers reappear; that is, all of the terms have the same values as for the angle 0°. Basically, the dependence in the range of the rotation angle from 30° to 60° is displayed in reverse order to that from 0° to 30°.

Our main conclusion is that the repulsion appeared as result of the interaction of two systems of closed electron shells whose lattices are superposed, is the central force controlling the efficiency of the interlayer orbital interactions. As the flake rotation breaks the lattice superposition, the suppression of the repulsion induces an improvement of orbital interactions (such as the electronic coupling) thereby lowering the bonding energy ΔE^0. Because the orbital interaction between the flakes depends on the flake rotation, the equilibrium distance d_{eq} also fluctuates with rotation. The modification of the equilibrium distance d_{eq} follows the dependence observed for the bonding energy ΔE^0 which is controlled by the Pauli repulsion. The maximum equilibrium distance $d_{eq} = 3.67$ Å is obtained for the AA stacking which is suppressed down to $d_{eq} = 3.43$ Å as the flakes are at an angle 18° that brings the system to the lowest energy state achievable with rotation. If the rotational angle grows further beyond 18°, the magnitude of d_{eq} enhances again and for $\theta \simeq 30°$ its value is 3.54 Å.

VI. DISCUSSION AND SUMMARY

Two graphene layers stacked in the AA pattern which is characterized by the lattice superposition between the layers is the most unstable configuration in the bilayer geometry. The instability appears as a result of strong interlayer repulsion induced by the interaction of the filled orthogonal π orbitals within the overlap region. Therefore, any minimal disruption of the lattice superposition lowers the total bonding energy and leads to an enhancement of the system stability. The AB stacking is the most successful scheme to suppress the Pauli repulsion because it

induces the maximum mis-orientation in the interlayer lattice order and therefore, the AB stacking appear to be the ground state of the system characterized by the strongest bonding interactions between the layers. However, an alternative way to induce the lattice mis-orientation from that superposed in the AA stacking and thereby, to transfer the system to the lower energy state is the layer rotation. It should be noted that any modification of the lattice order different from the AB stacking would be metastable (such as AA') because AB stacking is the ground state of the system.

For adjacent graphene flakes of finite size, the rotation of one flake relative to the other induces a fast reduction of the repulsive part (ΔE_p) and an increase of the attractive forces (orbital interaction energy ΔE_{oi}) such that both these tendencies lower the total bonding energy between the layers ΔE^0. The lowest bonding energy ΔE^0 is achieved for the rotation angle of $\theta \simeq 18°$. This state is still metastable but with the lowest value of the bonding energy among all the rotation angles, and its value correlates with that for the AB stacking being the ground state of bilayer graphene. However, as it was already noted above, the description of the adjacent graphene layers by the model system of finite flakes has crucial disadvantage caused by the underestimation of the interspot areas of the AB stacking into the interlayer repulsion. As we switch to the twisted bilayer graphene of infinite size, the contribution of large areas of AB stacking, which was largely neglected in the flake system, should be considered. For a small rotation angle the percentage of the AA spotted areas is large which decreases with angle enhancement. Thus, for an angle altered from 10° to 12°, a decrease of 2.5% of AA staking is observed.[29] Obviously, since the larger interspot areas of AB stacking is observed for small rotation angles 2−5° (see ref 29. for the images of various rotation structures), we would expect that the rotation angle of much smaller magnitude than that for the finite systems might be required ($\theta < 18°$) to bring the stacked graphene layers to the metastable state with the lowest energy.

However, additionally to rotation there is another way to make the system of the flakes stacked in the AA arrangement more stable, which is to raise the interlayer distance when the bonding energy is lowered again due to suppression of the Pauli repulsion between the layers (see Figure 1b). In the case of misoriented bilayer graphene exhibiting the Moiré pattern, the distribution of the repulsive forces would be nonuniform as the lattice order is not the same in different areas, i.e., a maximum force pushing apart two lattices would originate at the AA-spots of the lattice superposition. Moreover, another interesting distinction between the system of adjacent flakes and bilayer graphene of infinite size is the alteration of its rigidity. Recalling that the free-standing graphene is subjected to rippling of its surface,[30] the lower rigidity of the graphene layers than that of flakes is anticipated. Therefore, we expect that a strong Pauli repulsion which is pronounced locally at the center of the AA-spots might not able to modify the interlayer separation throughout the whole system because of large areas of AB stacking, but would rather induce a local lattice distortion forming the bump on the surface with its highest point at the center of the AA-spot.[18] To simulate this effect, the flake of larger size containing the bigger areas of AB stacking have been examined and already for that system the generation of the bump as high as 0.2 Å was observed. However, the bump height may be enhanced for an infinite system due to better efficiency of the attractive interactions in the interspot areas and lower rigidity of the layers. In fact, the appearance of

24672

dx.doi.org/10.1021/jp2095032 |*J. Phys. Chem. C* 2011, 115, 24666–24673

bumps can explain the brightening of the AA-spots observed in the STM images of the twisted bilayer graphene.[1−3]

Finally, we consider the interlayer coupling, which is found to be a function of the rotation angle and interlayer distance. As fragments being stacked, there are two types of π interactions occurs, such as perturbation of the occupied/occupied orbitals ($\pi−\pi$ interaction) and interaction of the occupied/unoccupied orbitals ($\pi−\pi^*$ interaction). According to the theoretical models developed to describe the behavior of the π bands in bilayer graphene, the modification of the linear dispersion of the Dirac cones to a parabolic one has been simulated by inclusion of the $\pi−\pi$ orbital interaction only.[9−27] However, we found that although the intrabands interactions play an important role, but in particular, the interbands part must be introduced in the model to account for the decoupling effect arising in the AA stacked graphene layers. The orbital interaction energy ΔE_{oi} is therefore suppressed at least five times as the lattice arrangement was changed from AB to AA, due to vanishing of the $\pi−\pi^*$ interactions between fragments, which is reflected by a drastic reduction of the spatial overlap integral $J_{i,j}^{H−L}$.

■ REFERENCES

(1) Varchon, F; Mallet, F.; Magaud, L.; Veuillen, J.-Y. *Phys. Rev. B* **2008**, *77*, 165415.

(2) Li, G.; Luican, A.; Lopes dos Santos, J. M. B.; Castro Neto, A. H.; Reina, A.; Kong, J.; Andrei, E. Y. *Nat. Phys.* **2009**, *6*, 109.

(3) Hass, J.; Varchon, F.; Millán-Otoya, J. E.; Prinkle, M. S.; Sharma, N.; de Heer, W. A.; Berger, C.; First, P. N.; Magaud, L.; Conrad, E. H. *Phys. Rev. Lett.* **2008**, *100*, 125504.

(4) Reina, A.; Jia, X.; Ho, J.; Nezich, D.; Son, H.; Bulovic, V.; Dresselhaus, M. S.; Kong, J. *Nano Lett.* **2009**, *9*, 30.

(5) Warner, J. H.; Rümmeli, M. H.; Gemming, T.; Büchner, B.; Briggs, G. A. D. *Nano Lett.* **2009**, *9*, 102.

(6) Shallcross, S.; Sharma, S.; Kandelaki, E.; Pankratov, O. A. *Phys. Rev. B* **2010**, *81*, 165105.

(7) Shallcross, S.; Sharma, S.; Pankratov, O. A. *Phys. Rev. Lett.* **2008**, *101*, 056803.

(8) Lopes dos Santos, J. M. B.; Peres, N. M. R.; Castro Neto, A. H. *Phys. Rev. Lett.* **2007**, *99*, 256802.

(9) McCann, E. *Phys. Rev. B* **2006**, *74*, 161403.

(10) Bolotin, K. I.; Sikes, K. J.; Jiang, Z.; Klima, M.; Fudenberg, G.; Hone, J.; Kim, P.; Stormer, H. L. *Solid State Commun.* **2008**, *146*, 351.

(11) Abergel, D. S. L.; Apalkov, V.; Berashevich, J.; Ziegler, K.; Chakraborty, T. *Adv. Phys.* **2010**, *59*, 261.

(12) Allen, M. J.; Tung, V. C.; Kaner, R. B. *Chem. Rev.* **2010**, *110*, 132.

(13) Latil, S.; Meunier, V.; Henrard, L. *Phys. Rev. B* **2007**, *76*, 201402.

(14) Dresselhaus, M. S.; Dresselhaus, G. *Adv. Phys.* **1981**, *30*, 139.

(15) Yoshizawa, K.; Yumura, T.; Yamabe, T.; Bandow, S. *J. Am. Chem. Soc.* **2000**, *122*, 11871. Yumura, T.; Yoshizawa, K. *Chem. Phys.* **2002**, *279*, 111. Yoshizawa, K.; Kato, T.; Yamabe, T. *Bull. Chem. Soc. Jpn.* **1998**, *71*, 2087.

(16) Ruuska, H.; Pakkanen, T. A. *J. Phys. Chem.* **2001**, *105*, 9541.

(17) Charlier, J.-C.; Gonze, X.; Michenaud, J.-P. *Europhys. Lett.* **1994**, *28*, 403.

(18) Berashevich, J.; Chakraborty, T. *Phys. Rev. B* **2011**, *84*, 033403.

(19) Grimme, S. *J. Comput. Chem.* **2004**, *25*, 1463.

(20) ADF2008.01, SCM, *Theoretical Chemistry*; Vrije Universiteit: Amsterdam, The Netherlands.

(21) Bickelhaupt, F. M.; Baerends, E. J. *Rev. Comp. Chem.* **2000**, *15*, 1.

(22) Senthilkumar, K.; Grozema, F. C.; Guerra, C. F.; Bickelhaupt, F. M.; Lewis, F. D.; Berlin, Y. A.; Ratner, M. A.; Siebbeles, L. D. A. *J. Am. Chem. Soc.* **2005**, *127*, 14894.

(23) Shamov, G. A.; Budzelaar, P. H. M.; Schreckenbach, G. *J. Chem. Theory Comput.* **2010**, *6*, 477.

(24) Senent, M. L.; Wilson, S. *Int. J. Quantum Chem.* **2001**, *82*, 282.

(25) Han, M. Y.; Özyilmaz, B.; Zhang, Y.; Kim, P. *Phys. Rev. Lett.* **2007**, *98*, 206805.

(26) Berashevich, J.; Chakraborty, T. *Phys. Rev. B* **2009**, *80*, 115430.

(27) Zhang, F.; Sahu, B.; Min, H.; MacDonald, A. H. *Phys. Rev. B* **2010**, *82*, 035409.

(28) Bills, J. L.; Snow, R. L. *J. Chem. Educ.* **1982**, *59*, 142.

(29) Campanera, J. M.; Savini, G.; Suarez-Martinez, I.; Heggie, M. I. *Phys. Rev. B* **2007**, *75*, 235449.

(30) Fasolino, A.; Los, J. H.; Katsnelson, M. I. *Nat. Mater.* **2007**, *6*, 858.

24673

dx.doi.org/10.1021/jp2095032 |*J. Phys. Chem. C* 2011, 115, 24666–24673